Cell Communication and Signaling

RESEARCH Open Access

The dose-dependent dual effects of alpha-ketoglutarate (AKG) on cumulus oocyte complexes during in vitro maturation

Yunjie Liu[1], Xin Xiao[1], Likai Wang[1], Yao Fu[1], Songyang Yao[1], Xuening Liu[1], Boda Chen[1], Jiarui Gao[1], Yaying Zhai[1], Zixia Shen[1], Laiqing Yan[1], Yiwei Wang[1], Pengyun Ji[1], Bingyuan Wang[1] and Guoshi Liu[1*]

Abstract

In this study, we reported for the first time the dose-dependent dual effects of Alpha-Ketoglutarate (AKG) on cumulus oocyte complexes (COCs) during in vitro maturation (IVM). AKG at appropriate concentration (30 μM) has beneficial effects on IVM. This includes improved cumulus expansion, oocyte quality, and embryo development. These effects are mediated through multiple underlying mechanisms. AKG reduced the excessive accumulation of reactive oxygen species (ROS) in cumulus cells, reduced the consumption of GSH and NADPH. Cumulus GSH and NADPH were transported to oocytes via gap junctions, thereby reducing the oxidative stress, apoptosis and maintaining the redox balance in oocytes. In addition, AKG improved the mitochondrial function by regulating the mitochondrial complex 1 related gene expression in oocytes to maintain mitochondrial membrane potential and ATP production. On the other hand, oocyte generated GDF9 could also be transported to cumulus cells to promote cumulus expansion. Conversely, a high concentration of AKG (750 μM) exerted adverse effects on IVM and suppressed the cumulus expansion as well as reduced the oocyte quality. The suppression of the cumulus expansion caused by high concentration of AKG could be rescued with GDF9 supplementation in COCs, indicating the critical role of GDF9 in IVM. The results provide valuable information on the variable effects of AKG at different concentrations on reproductive physiology.

*Correspondence:
Guoshi Liu
gshliu@cau.edu.cn

Full list of author information is available at the end of the article

Graphical abstract

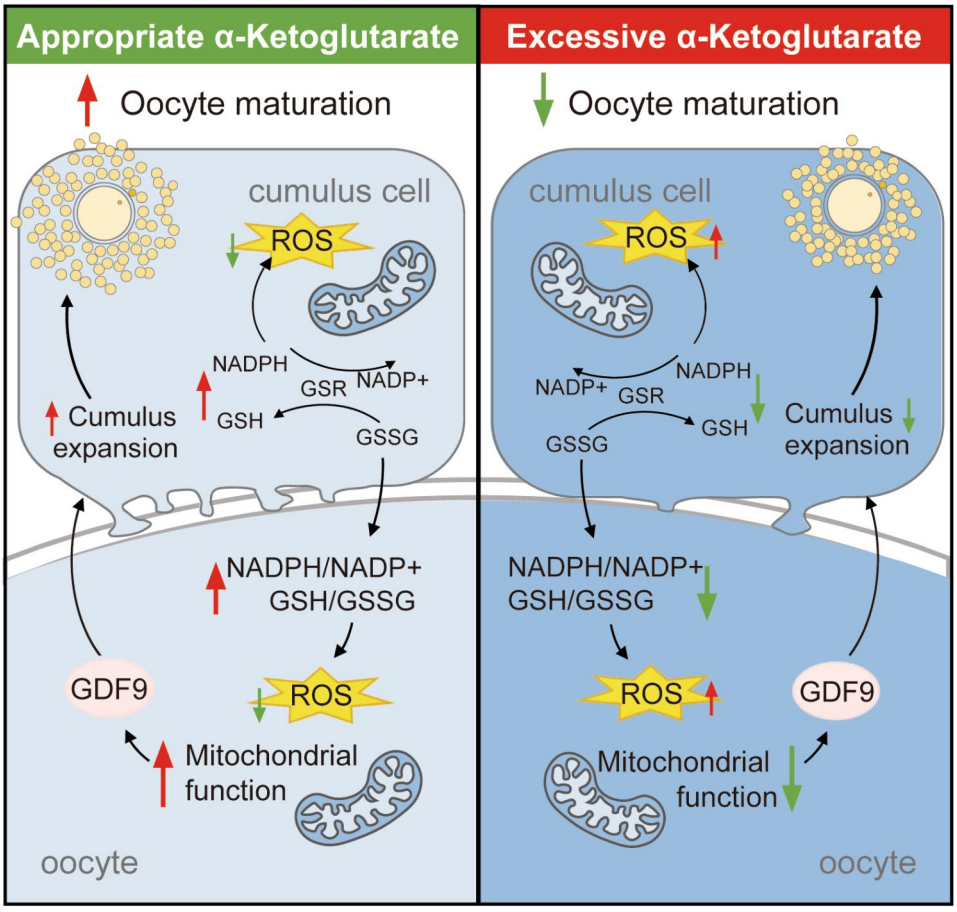

Keywords Alpha-ketoglutarate, Cumulus oocyte complexes, In vitro maturation, Reactive oxygen species, Cumulus cells-oocyte communication

Introduction

Advancements in in vitro embryo production technology have significantly enhanced reproductive efficiency in domestic animals. In both domestic animals and humans, the number of embryos obtained through in vitro embryo production constantly increases annually [1]. For example, in 2022, the cow in vitro produced (IVP) embryos accounted for 80.4% of all transferrable cattle embryos globally [2]. The oocyte maturation in the in vitro culture condition is the first step in the in vitro embryo production. However, significant differences between in vitro and in vivo environments lead to a reduction in oocyte quality, inhibiting embryo development and implantation [3, 4].

Physiologically, the oocytes and cumulus cells form a cumulus-oocyte complex, and their coordinated crosstalk determines the developmental ability of oocytes, the fertility and the outcomes of assisted reproductive therapy [5]. It is well known that the antioxidant capacity of oocytes is relatively weak and they primarily rely on the cumulus cells to provide antioxidative defense for them [6]. The communication between cumulus-oocytes is mainly mediated by the gap junctions and transzonal projections (TZPs) [7]. Several basic metabolic processes of oocytes depend on the support of cumulus cells. For example, the oocytes require the supply of glutathione (GSH), NAPDH, pyruvate and other substances from cumulus cells to maintain their energy metabolism and antioxidant defense [8]. GSH is the primary endogenous antioxidant in oocytes, which effectively removes excessive ROS to protect cells [9]. Maintaining a balance between ROS and GSH is critical for normal cellular function [10]. GSH is either synthesized from glutamate and cysteine by glutamate cysteine ligase (GCL) or regenerated from oxidized glutathione disulfide (GSSG) by glutathione reductase (GSR). GSR requires NADPH as a

co-substrate to convert GSSG to reduced GSH; therefore, NADPH is directly related to GSH synthesis [11]. Conversely, oocytes also contribute to the metabolic activity of cumulus cells. The oocyte-secreted factors (OSFs) including growth differentiation factor 9 (GDF9) [12, 13] and bone morphogenetic protein 15 (BMP15) [14] are necessary for the proliferation and expansion of cumulus cells.

Alpha-Ketoglutarate (AKG) is a key metabolite in the tricarboxylic acid cycle (TCA cycle) [15]. Recent studies have found that it has important anti-aging function [16]. AKG maintains mitochondrial metabolic homeostasis [17], promotes mitophagy and inhibits ROS production [18]. The concentration of AKG in the preovulatory follicular fluid of cows is positively correlated with follicle diameter [19]. This follicle diameter is also positively associated with pregnancy rate and embryo survival rate [20]. Previous studies have found that AKG supplementation promotes oocyte maturation and subsequent embryonic development in pigs [21] and mice [22], and improves the quality of mice blastocysts in vitro, as well as increases the number of inner cell mass cells and the rate of implantation [23]. In oocytes matured in vitro, AKG increased GSH levels and reduced ROS accumulation and apoptosis [24]. However, the signaling pathways of AKG on oocyte maturation in the in vitro condition have not been clarified. In this study, we examined the effects of varying doses of AKG on cumulus-oocyte crosstalk under in vitro conditions. Our results showed that the appropriate dose of AKG enhanced cumulus-oocyte crosstalk and inhibited oxidative stress. However, high levels of AKG inhibited OSF secretion and increased oxidative stress in the cumulus-oocyte complex.

Materials and methods

Chemicals

All chemicals and reagents, unless specified, were purchased from Sigma-Aldrich Chemical Co (Co.St.Louis, USA). The goat anti-Rat IgG (H+L) Cross-Adsorbed Secondary Antibody, DAPI solution were purchased from Invitrogen (CA, USA). HRP-conjugated Affinipure Goat Anti-Rabbit IgG (H+L) was from Proteintech (Beijing, China).

In vitro embryo production

Cow ovaries were collected from the slaughterhouse and transported to the laboratory in the container at 35 ℃ for the subsequent operations within 2 h. The ovaries were carefully washed, and follicular fluid was aspirated using a syringe. Cumulus-oocyte complexes (COCs) were then isolated using the tip of a glass tube. In certain experiments, germinal vesicle (GV) oocytes were obtained by vortexing and treating with 0.3% hyaluronidase treatment to remove cumulus cells. GV oocytes or COCs were cultured in maturation medium (IVF-bioscience, New York, USA) at 38.5℃ and 5% CO2 with maximum humidity for 21–22 h. The polar body extrusion (PBE) rate was counted. For AKG supplementation study, GV oocytes or COCs were cultured in maturation medium containing various concentrations of α-Ketoglutaric acid (AKG) (Sigma, CA, USA). Based on our unpublished observations, the concentrations of AKG in cow follicles of different sizes (0.2–2 cm) are in the range of 1–5 μM. According to the pre-experiment in the early stage, we determined 30, 150 and 750 μM as the supplementary dose for the subsequent experiment. In some experiments, the culture medium was supplemented with 100 ng/mL GDF9 protein (MCE, Shanghai, China) or 1 μM carbenoxolone disodium (CBX) (MCE, Shanghai, China). AKG, GDF9 and CBX were dissolved in M199 solution and diluted with a maturation medium to obtain the desired final concentrations. Control groups were treated with the same amount of M199 solution.

In order to explore whether AKG supplementation during IVM can affect IVP efficiency, in vitro fertilization and embryo culture were performed. Frozen semen of dairy cows from Beijing dairy center was thawed in 37 ℃ warm water bath and the fertilization culture medium were added, then, centrifuged twice to remove the semen diluent, thereafter, the sperm was diluted to 2×10^6 sperms/ml in fertilization culture medium in a 35 mm Petri dish. Matured COCs were transferred to the Petri dished, co-incubated with the sperm for 12 h. After fertilization, the fertilized oocytes were gently pipetted to remove the surface adherent sperm and transferred to the development medium and cultured in the incubator at 38.5 ℃, 5% CO_2, 90% N_2 saturated humidity. Embryo cleavage rates were assessed after 2 days, and blastocyst development rates were recorded after 7 days.

Estimation of cumulus expansion

The ability of AKG to regulate cumulus expansion was analyzed by adding 30, 150 and 750 μM AKG to the COCs in vitro culture medium. Before and after IVM, we photographed the COCs and measured the area of each. However, since it was not possible to match COCs before and after IVM on a one-to-one basis, we calculated the relative area by subtracting the total area of each group of 10 COCs from their initial total area. The cumulus cell expansion index (CEI) was calculated using a previously described scale [25]. Briefly, the CEI scale ranges from 0 to 4: a grade of 0 indicates no cumulus expansion; a grade of 1 indicates only the outermost 1–2 cumulus granulosa cells expanded; a grade of 2 indicates expansion of the outer half of the cumulus cells expanded; a grade of 3 indicates the corona radiata did not expand, but the rest were expanded; a grade of 4 indicates all cumulus cells expanded.

Immunofluorescence assay

The blastocysts obtained from in vitro culture were washed in PBS containing 0.1% PVA, respectively incubated in 4% PFA for 6 h, 0.5% TirtonX-100-PBS for 1 h and 3% BSA-PBS for 2 h. Subsequently, Sox2 antibody (14-9811-82, eBioseience, CA, USA) was diluted in 3% BSA-PBS at a ratio of 1:500 and the embryos were incubated at 4° C for 8 h. After incubation, excess antibody was washed with 0.5% TritonX-100-PBS, and the embryos were incubated with a fluorescent-labeled secondary antibody diluted 1:500 in 0.5% TritonX-100-PBS in the dark for 1 h. Following a PBS wash, the anti-fluorescence quenching blocking agent containing DAPI was applied, and samples were covered with a cover slip and observed using a confocal microscope (ANDOR-BC43, OXFORD). Channel 405 (for DAPI) and 647 (for Sox2) were used, and images were captured with default parameters and settings. In the image, DAPI (blue) labeled the nuclei of all blastocyst cells, and Sox2 (yellow) was specifically expressed in the inner cell mass (ICM) cells. The number of cells stained with blue and yellow fluorescence in each blastocyst was counted to determine the total number of cells and the number of ICM cells in the blastocyst.

Evaluation of cortical granules (CGs) dynamics

Cortical granules are synthesized in the center of the oocyte and translocated to the cortex and remain positioned several microns below the plasma membrane until fertilization. In order to evaluate the effect of AKG on the maturation of oocytes, after 22 h of in vitro maturation, oocytes were treated with 0.5% pronase at 37 ℃ for 5 min to remove the zona pellucida. Denuded oocytes were fixed in 4% PFA for 30 min, followed by incubation in PBS containing 3 mg/ml BSA and 7.5 mg/ml glycine for 15 min. Oocytes were then permeabilized in PBS containing 0.5% TritonX-100 for 30 min. To visualize cortical granules, oocytes were stained with 100 μg/ml FITC-conjugated Lectin from Arachis hypogaea for 30 min at room temperature.

Samples were observed under a microscope using the 488 nm channel, and images were captured with default parameters and settings. The fluorescence intensity near the plasma membrane was analyzed using ImageJ software. Oocytes were represented as circle A, and the total fluorescence intensity and area of circle A were measured. A concentric circle B was drawn in the region of lower fluorescence intensity inside the oocyte, and the total fluorescence intensity and area of circle B were recorded. Ensure that the radius difference of each statistical oocyte A and B is the same. The average fluorescence intensity of the outer part of the oocyte = (Total fluorescence intensity of A - Total fluorescence intensity of B) / (Area of A - Area of B).

Evaluation of cytoskeleton assembly

F-actin polymerization abilities were positively related to the cytoplasmic maturation level of mammalian oocytes. In order to evaluate the effect of AKG on the maturation of oocytes, after 22 h of in vitro maturation, oocytes were incubated in 0.5% pronase at 37 ℃ for 5 min to remove the zona pellucida. Denuded oocytes were fixed in 4% paraformaldehyde (PFA) for 30 min, followed by incubation in PBS containing 0.5% TritonX-100 for 30 min. Oocytes were then transferred to PBS with 1% BSA for 30 min. Alexa Fluor Plus 555 Phalloidin (Invitrogen, CA, USA) was used to stain the samples for 60 min at room temperature. Phalloidin can selectively label F-actin. Fluorescence intensity of each oocyte was analyzed under a microscope using ImageJ software. Samples were observed using the 555 nm channel, and images were captured with default settings. Fluorescence intensity near the plasma membrane was quantified using ImageJ. Briefly, total cell fluorescence intensity was measured, and the intensity from the central region was subtracted to calculate the fluorescence intensity near plasma membrane.

Measurement of ROS level in COCs

To investigate whether AKG supplementation affects ROS levels in oocytes and cumulus cells within COCs, the ROS levels in oocytes was first assessed. 2'-7'dichlorofluorescin diacetate (DCFH-DA) is a fluorogenic dye that measures ROS activity. DCFH-DA itself has no fluorescence and can freely cross the cell membrane. After cellular uptake, DCFH-DA is deacetylated by cellular esterases to a non-fluorescent compound, which is later oxidized by ROS into 2'-7'dichlorofluorescein (DCF). DCF is a fluorescent compound with a maximum excitation and emission spectra of 495 nm and 529 nm respectively. Oocytes were treated with 0.5% pronase at 37 ℃ for 5 min to remove the zona pellucida. After washing with PBS, the oocytes were stained with 10 μM DCFH-DA (Solarbio, Beijing, China) at 37 ℃ for 20 min, the oocytes were washed three times with PBS, and observed under a fluorescence microscope and channel 488 was used. The fluorescence intensity of each oocyte was calculated using ImageJ software.

For cumulus cells, cells were washed once with PBS, and stained with 10 μM DCFH-DA in the dark at 37 °C for 20 min. The cells were washed three times with PBS, the cells were analyzed by flow cytometry (FACSCalibur, Becton Dickinson Co. NJ, USA). At least 10,000 events of single cells per sample were collected, and data were analyzed using FlowJo software. Cells were gated based on forward scatter (FSC) and side scatter (SSC) parameters, and a histogram was generated to show DCFH-DA intensity for the gated population.

Cell apoptosis analysis in COCs

To investigate whether AKG supplementation affects the apoptosis of oocytes and cumulus cells in COCs. For oocytes, denuded oocytes were stained with Annexin V/FITC 1:20 (Annexin V/FITC; Solarbio, China) in the dark at room temperature for 5 min. The oocytes were then washed three times with PBS, observed under a fluorescence microscope and channel 488 was used. The fluorescence intensity near the plasma membrane of each oocyte was calculated using ImageJ software.

For cumulus cells, they were washed once with PBS and stained with 0.1mL of Annexin V/FITC diluted in PBS in the dark at room temperature for 5 min. Then propidium iodide solution (PI) and 400 μL of PBS were added for immediate flow cytometry analysis. Two additional samples were prepared, which served as a positive control for single staining of Annexin V or PI, respectively. A minimum of 10,000 single-cell events were collected per sample. Depending on the fluorescence intensities of Annexin V and PI, the cell populations can be distinguished into Viable cells (Annexin V/PI−−), Early apoptotic cells (Annexin V/PI+−), and Late apoptotic cells (Annexin V/PI++).

Assessment of mitochondrial distribution and mitochondrial membrane potentials (MMP) in oocytes

To evaluate the mitochondrial distribution, denuded oocytes were stained with 20nM mitotracker (mitotracker red, invitrogen, CA, US) in the dark at 37 ℃ for 20 min. After staining, the oocytes were washed with PBS, fixed in 4% PFA for 30 min, and mounted onto glass slides. The oocytes were observed under a confocal microscope, uneven fluorescence was considered as abnormal distribution.

To measure the mitochondrial membrane potentials (MMP), cumulus cells isolated from COCs were stained using the JC-1 mitochondrial membrane potential assay kit (Solarbio, Beijing, China) following manufacturer's instructions. Briefly, cumulus cells were stained with diluted JC-1 staining solution in the dark at 37 ℃ for 20 min and washed three times with the staining buffer, then, the pronase was added to remove the zona pellucida of oocytes to avoid the adsorption of dye particles on the zona pellucida. Thereafter, the cumulus cells were washed with PBS and observed under a fluorescence microscope, channel 488 and 555 was used. The red (J-aggregates) fluorescence intensity and green (monomer) fluorescence intensity in oocytes were counted in ImageJ software, and their ratio was used to determine MMP levels.

GSH/GSSG, NADP+/NADPH and ATP analysis

Cumulus cells and oocytes were separately isolated from COCs. For oocytes, the zona pellucida was removed. For cumulus cells, hyaluronidase was added to digest the junctions between cumulus cells to obtain single-cell suspensions and the blood cell counting plate was used to count the cell number. The GSH/GSSG, NADP+/NADPH and ATP levels of oocytes and cumulus cells were detected with the detection kits (GSH and GSSG Assay Kit, Beyotime, Shanghai, China) (NADP+/NADPH Assay Kit with WST-8, Beyotime, Shanghai, China) (Enhanced ATP Assay Kit, Beyotime, Shanghai, China) respectively, following the manufactures' instructions. For GSH/GSSG, the absorbance was measured at 412 nm, for NADP+/NADPH, the absorbance was measured at 450 nm, and the chemiluminescence mode was used to detect the ATP content (Infinite F200, Tecan Life Sciences).

Analysis of gap junctions of cumulus cell-oocyte

Analysis of gap junctions was performed according to the previously reported method [26]. Briefly, the COCs were cultured in the maturation medium for different times (3, 6, 9, 12, 15, 18, 21 h) and were pulsed with 1μM Calcein-AM (Beyotime, Shanghai, China), and then incubated at 37 ℃ for 15 min. The excessive dye was cleaned. The surrounding cumulus cells were denuded and avoided light exposure at 37 ℃ for 30 min to let the dye be better combined. The samples were analyzed under a fluorescence microscope and photographed, the fluorescence intensity in oocytes was evaluated using ImageJ software.

Transzonal projections (TZPs) analysis

TZPs analysis was performed according to the previously reported methods [27], Briefly, COCs were cultured in maturation medium for different durations (9, 12, 15, 18, 21 h), fixed in 4% PFA for 30 min, and then incubated with PBS containing 0.5% TritonX-100 for 30 min, and transferred into PBS containing 1% BSA for additional 30 min. TZPs were stained using Alexa Fluor Plus 555 Phalloidin (Invitrogen, CA, USA) at room temperature for 60 min. Following staining, samples were observed under a microscope. TZPs, which form connections between cumulus cells and oocytes and are located on the zona pellucida, were quantified based on fluorescence intensity using ImageJ software.

qPCR

Total RNA in cumulus cells was extracted with TRIzol reagent (Vazyme, Nanjing, China). Hiscript III Reverse Transcriptase (Vazyme, Nanjing, China) were used in first-strand cDNA synthesized. Primers were designed using Primer Premier software. The primer sequences are as follows: (*ACTB*: F-ATCGTCCACCGCAAATGCTTCT, R-GCCATGCCAATCTCATCTCGTT; *HAS2*: F-TCTCTAGAAACCCCCATTAAGTTG, R-ATCTTCCGAGTTTCCATCTATGAC; *PTX3*: F-TGGCCTTGTGGGTAA

ATGGT, R-AGCCGTTCTTTTCTTGCCCA; *CD44*: F-CCTCGGATACCAGAGACTACG, R- CACACCTTCT CCTACTGTTGAC; *HMMR*: F- CTGTTTGATTCCTG GGTGTTTGA, R- GAGAGGAGGGCAGGGACAAT). Quantitative real-time PCR was performed in the Real-Time Thermal Cycler CFX96 (Bio-Rad, CA, USA). The procedure as follows: initial denaturation for 30s at 95 °C and 40 cycles of 5s at 95 °C, annealing for 5s at 60 °C and elongation at 72 °C for 5s. Relative expression values wereobtained using the average of three reference genes and the $2^{-\Delta\Delta CT}$ method.

Western blot analysis

For cumulus cells, cells were washed with ice-cold PBS, treated with ice-cold RIPA lysis buffer (Beyotime, Shanghai, China) with 1 mM phenylmethylsulfonylfluoride (PMSF) for 30 min. Then the cells were centrifuged at 12 000× g at 4 °C for 5 min. The supernatant was aspirated, the SDS loading buffer was added and, then, the sample was heated at 100 ℃ for 10 min. For oocytes, after denudation of cumulus cells from COCs, The oocytes were added to the lysis buffer(2×Laemmli Sample Buffer (Bio-Rad, CA, US)+5% 2-Mercaptoethano+1% PMSF) and heated at 100 ℃ for 10 min. Protein was loaded by 12% SDS-PAGE and transferred to the PVDF membranes. Then, the membranes were blocked with 5% BSA and incubated with antibodies of GDF9 (273455, Abcam, MA, USA), HAS2 (115388, Invitrogen, CA, USA), NDUFS4 (15849, Proteintech, Wuhan, China) and NDUFB9 (15572, Proteintech, Wuhan, China), respectively. Finally, the membranes were detected using the SuperSignal™ West Pico PLUS ECL chemiluminescence reagent (Thermo Scientific; MA, USA). Chemiluminescence was visualized using an Amersham ImageQuant 800 RT-ECL camera (GE Healthcare).

RNA-Seq and enrichment analysis

For oocytes, after denuding the excess cumulus cells and zona pellucida, 10 oocytes were collected for each sample, and the full-length mRNA was extracted by using Single Cell Full Length mRNA-Amplification Kit (Vazyme, Nanjing, China). The sequencing library was constructed by using TruePrep DNA Library Prep Kit V2 (Illumina, Vazyme, Nanjing, China) following the manufacturer's instructions. After passing the quality inspection, sequencing was performed on the HiSeqX platform. For cumulus cells, RNA was extracted by Trizol method after cumulus cells were collected, and the library was constructed and sequenced on HiSeqX platform. Fastp 0.20.1 [28] and FastQC 0.11.9 [29] were used for data quality control. The bovine reference genome (Bos_taurus.ARS-UCD1.3.) and genome annotation (Bos_taurus Ars-ucd1.2.108) were read alignment with data using STAR 2.7.9a [30] software. Featurecounts software (Subread 1.6.3 [31]) performed gene counting, and DESeq2 [32] was used to analyze differential genes. Genes exhibited significant differences ($P<0.05$) were screened and for GO enrichment analysis with gProfiler [33].

Cell communication analysis

Cellchat [34] (version 2.1.0, R package) was used to evaluate the cell-cell interactions between cumulus and oocyte in different datasets. The recommended preprocessing functions were applied to analyze single or multiple datasets with default parameters. CellChatDB.human was used as a database for inferring cell–cell communication. All categories of ligand-receptor interactions in the database were used for analysis. Function netVisual_bubble can identify the up-regulated (increased) signaling ligand-receptor pairs in 30μM AKG group dataset compared to the control dataset.

Statistical analysis

Unless otherwise specified, all values were presented as mean±SEM. The ANOVA was used for the statistical analysis of the data followed by the 2-tailed unpaired T-test to compare the differences between the related two groups. All the analyses were performed using SPSS's (SPSS Inc., CA, USA). A p value less than 0.05 ($P<0.05$) was considered as statistically significant. $^{*}P<0.05$, $^{**}P<0.01$.

Result

Effects of different concentrations of AKG on oocyte maturation

The results showed that in the in vitro culture condition, AKG at 30 μM concentration significantly increased the polar body extrusion (PBE) rate of oocytes (Fig. 1D) and the degree of cytoskeleton assembly (Fig. 1E, F) in comparison to the control group. Following in vitro fertilization, the embryonic development and cleavage rates of these oocytes were markedly improved (Supplementary Fig. S1A-B). Although no significant differences were observed in blastocyst development efficiency or total cell number (Supplementary Fig. S1C, F), the number of inner cell mass (ICM) cells in the blastocysts was significantly higher in the AKG group compared to controls (Supplementary Fig. S1E). Since the ICM cell count is a key marker of blastocyst quality, these findings suggest that 30 μM AKG significantly improved oocyte maturation and subsequent blastocyst quality. However, supplementation with 750 μM AKG led to a significant reduction in cumulus expansion (Fig. 1A-C) PBE rate (Fig. 1D), and cortical granules (CGs) dynamic (Fig. 1G), indicating a detrimental impact on oocyte maturation. Moreover, 150 μM AKG supplementation showed no significant effect on in vitro matured oocytes (Fig. 1).

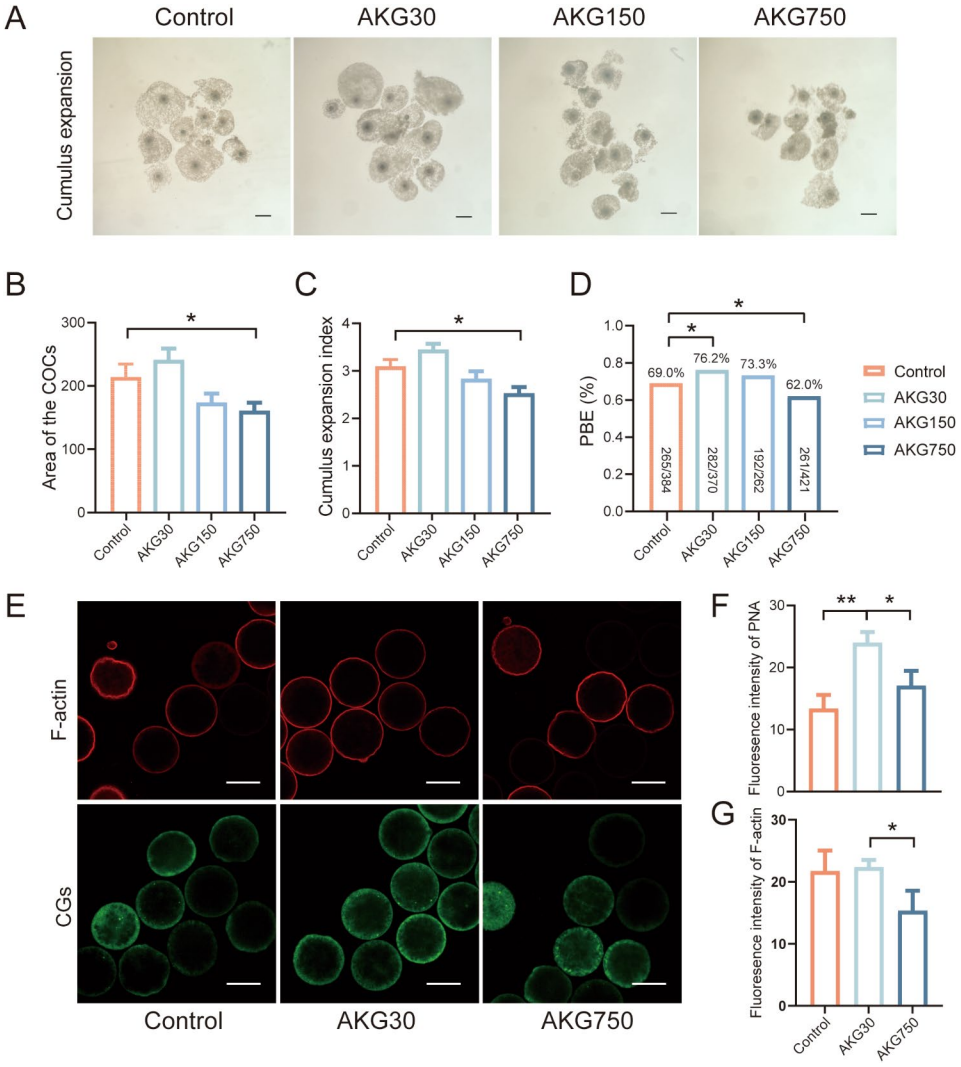

Fig. 1 Effect of different concentrations of AKG on oocyte maturation. **(A)** Representative images showed the cow cumulus oocyte complex after 22 h of culture with different concentrations of AKG treatments, Scale bar = 200 μM, $n = 31$ (Control), 30 μM AKG $n = 30$ (AKG30), 150 μM AKG $n = 31$ (AKG150), 750 μM AKG $n = 31$ (AKG750) examined over three independent experiments. **(B)** Relative cumulus expansion area. **(C)** Cumulus expansion index. **(D)** The polar body extrusion (PBE) rate of oocytes after 22 h of maturation. The number inside each bar indicates the number of PBE oocytes/total oocytes. Data were analyzed using the Chi-squared test with SPSS. **(E)** Representative images of cytoskeleton staining of oocytes labeled with F-actin and the CGs dynamic staining with Lectin from Arachis, Scale bar = 70 μM, $n = 23$ (Control), $n = 26$ (AKG30), $n = 23$ (AKG750) examined over three independent experiments. **(F)** Degree of cytoskeleton assembly of oocytes, as measured by the relative fluorescence intensity of F-actin in the outer layer of oocytes. **(G)** Degree of cortical granules (CGs) dynamic in oocytes, determined by the relative fluorescence intensity in the outer layer of oocytes

Effects of AKG on the ROS levels and apoptosis in COCs

To determine whether AKG affects cellular physiological functions through apoptosis and oxidative stress, we selected COCs from the 30 μM AKG and 750 μM AKG treatment groups, which had differing effects on oocyte maturation. Oocytes and cumulus cells were stained for apoptosis using Annexin V/Propidium iodide (PI) and for ROS levels using 2′,7′-dichlorofluorescin diacetate (DCFH-DA). The results showed that in the cumulus cells, 30 μM AKG supplementation significantly reduced ROS levels (Fig. 2A, B) and decreased the proportion of late apoptotic cells compared to the control (Fig. 2C-F). On the contrary, ROS content was significantly increased in 750 μM AKG treated group compared to the control (Fig. 2A, B). In oocytes, 30 AKG treatment similarly reduced ROS levels and apoptosis as observed in cumulus cells (Fig. 2G, H). Conversely, 750 μM AKG treatment resulted in increased ROS levels and apoptosis, similar to the effects observed in cumulus cells (Fig. 2I, J).

Effects of AKG on NADPH and GSH levels in cumulus cells and their transportation to oocytes via gap junctions

Cumulus-oocyte gap junction communication transmits metabolites (including ROS scavengers) between two types of cells. Given that AKG exerts similar effects on both cumulus cells and oocytes, we hypothesized that

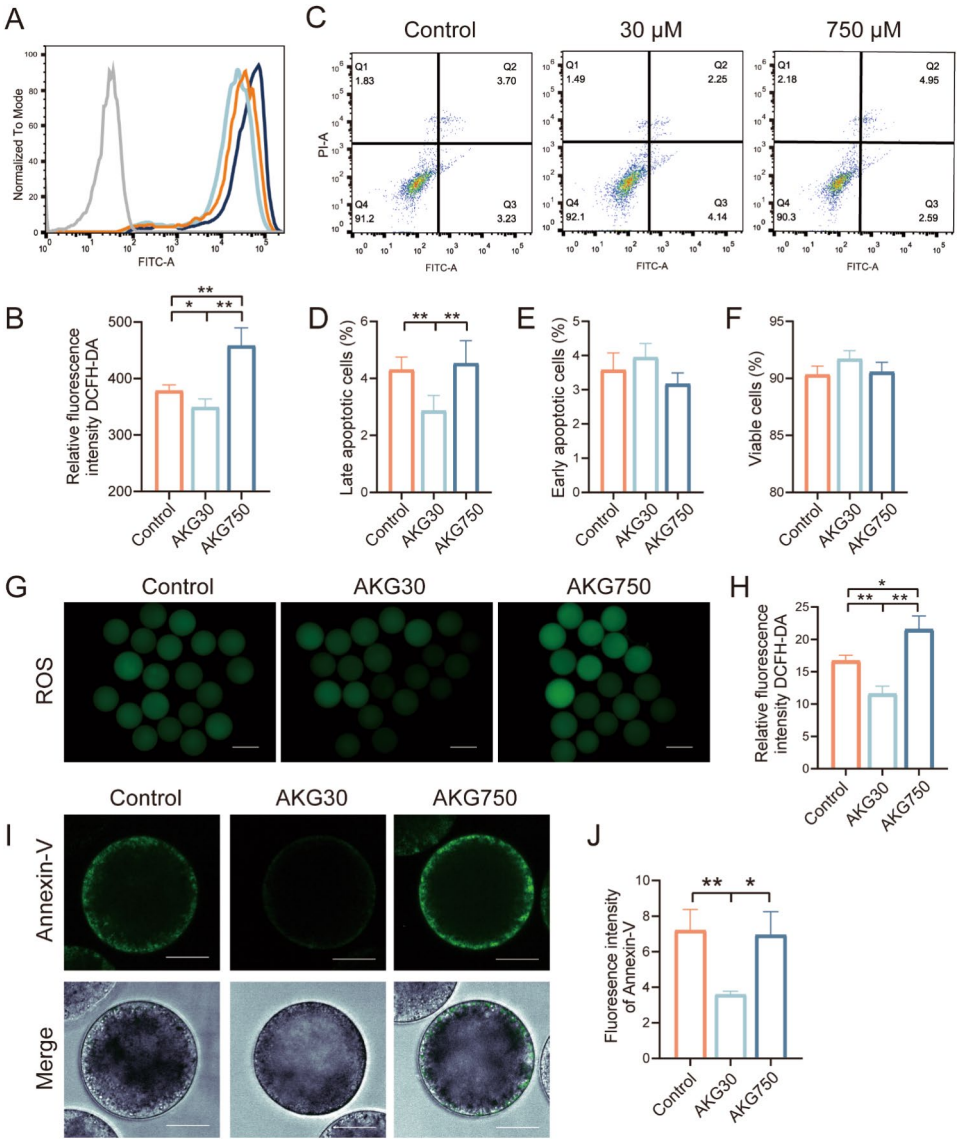

Fig. 2 Effects of AKG on the levels of ROS and apoptosis in cumulus cells and oocytes. **(A)** Representative images of the ROS levels detected by flow cytometry after cumulus cells were treated with different doses of AKG, $n=5$. **(B)** Bar graphs showed the quantification of ROS levels. **(C)** The original graph of Flow cytometry of Annexin/PI double stained of cumulus cells. The graph showed live cells in Q4, early apoptotic cells in Q3, late apoptotic cells in Q2. **(D)** Bar plots show population of viable (annexin V−/PI−), **(E)** early apoptotic (annexin V+/PI−), **(F)** late apoptotic (annexin V+/PI+) and **(G)** necrotic (annexin V−/PI+) cells. (H) Representative images of DCFHDA staining in control ($n=30$), AKG30 ($n=31$), and AKG750 ($n=29$), Scale bar = 100 μM. **(I)** Bar graphs showed the quantification of ROS levels. **(J)** Representative images of Annexin-V staining apoptotic status in control ($n=25$), AKG30 ($n=25$), and AKG750 ($n=30$), Scale bar = 40 μM. (K) Bar graphs showed the quantification of apoptosis levels

AKG influences NADPH and GSH production in cumulus cells, subsequently transporting them to oocytes via gap junctions. This hypothesis was tested by the addition of the gap junction inhibitor CBX. Transcriptome sequencing of cumulus cells in COCs treated with 30 μM and 750 μM AKG revealed upregulated expression of the oxoglutarate dehydrogenase (*OGDH*) gene at both concentrations. In cumulus cells treated with 750 μM AKG, the expression of the glutathione reductase (*GSR*) gene was significantly reduced (Fig. 3A), whereas no notable effect was observed in oocytes compared to the control (Fig. 3B). In addition, both GSSG and NADP+levels in cumulus cells and oocytes treated with 30 μM AKG were significantly decreased, accompanied by increases in the GSH/GSSG (Fig. 3C-E) and NADPH/NADP+ ratios (Fig. 3F-H). In contrast, the 750 μM AKG treatment group exhibited significantly opposite changes in all these parameters compared to the 30 μM AKG group. However, when the gap junction inhibitor CBX was added, AKG supplementations at both concentrations lost its ability to alter the GSH/GSSG and NADPH/NADP+ratio in the oocytes. This confirms that NADPH

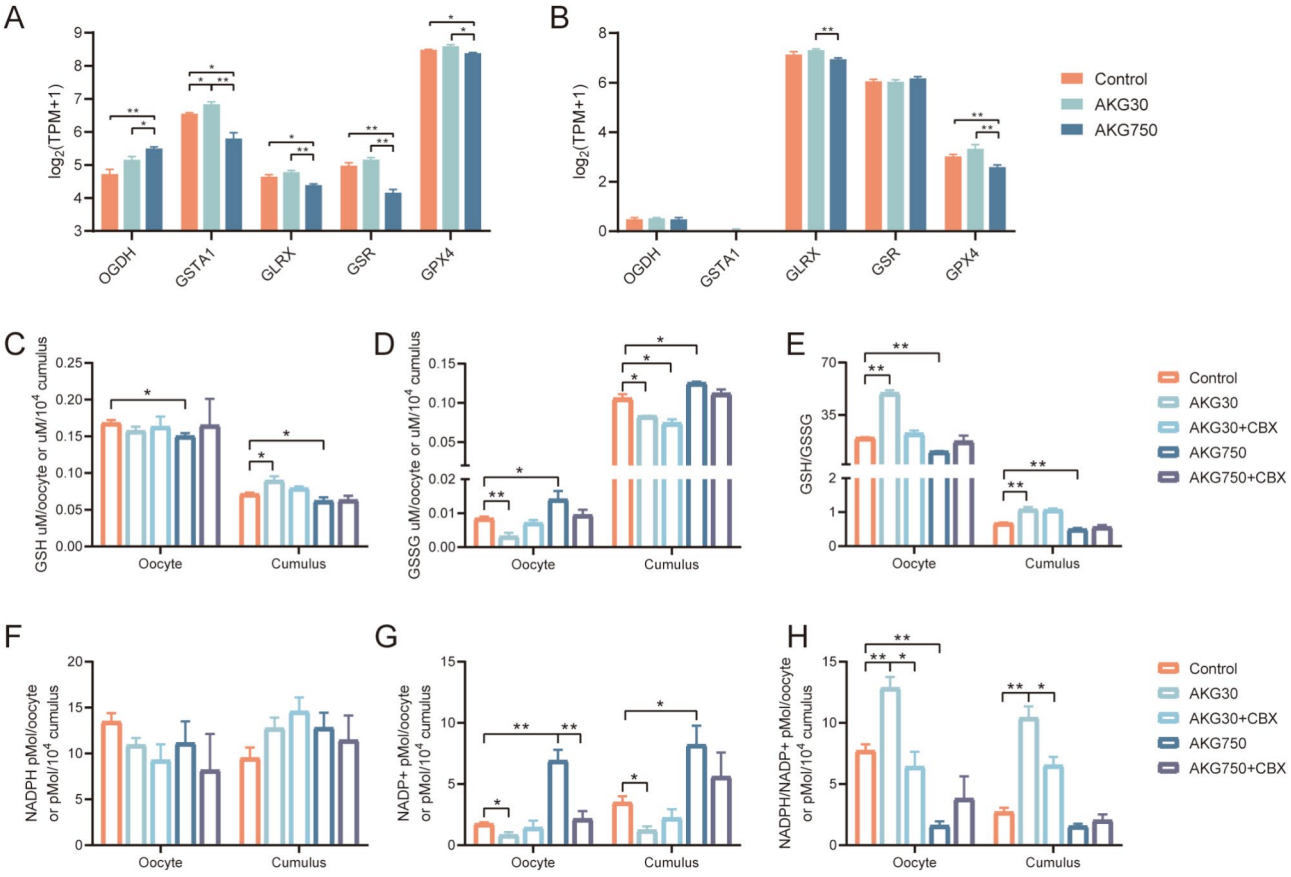

Fig. 3 Effects of AKG on GSH and NADPH in cumulus cells and oocytes **(A)** The expressions of target genes in cumulus cells expressed by $\log_2$ (TPM + 1), $n = 3$. **(B)** The expressions of target genes in oocytes expressed by $\log_2$ (TPM + 1), $n = 8$. **(C-E)** The levels of GSH, GSSG and GSH/GSSG in cumulus cells and oocytes of COCs, normalized to the content in one oocyte or 10^4 cumulus cells, $n = 3$. **(F-H)** NADPH, NADP+, NADPH /NADP + levels in cumulus cells and oocytes in COCs, normalized to the content in one oocyte or 10^4 cumulus cells, $n = 3$

and GSH produced in cumulus cells under AKG treatment were transported to oocytes via gap junctions.

Effects of AKG on mitochondrial distribution and function in oocytes

Given that ROS accumulation can lead to abnormal mitochondrial function, and AKG is a key metabolite in the TCA cycle, we investigated mitochondrial function, including mitochondrial distribution, ATP levels, and mitochondrial membrane potentials (MMP). Results showed that treatment with 30 μM AKG significantly increased the ATP production and MMP. In contrast, 750 μM AKG led to increased abnormal mitochondrial distribution and reduced ATP production, with no significant effect on MMP compared to the control group (Fig. 4A-E). GO enrichment analysis on genes with significant differences between the AKG at 30 μM vs. control group and AKG at 750 μM vs. control group was performed, respectively. The analysis showed that mitochondrial respiratory chain complex I (complex I), also known as NADH dehydrogenase complex assembly term, was significantly enriched in the up-regulated gene list in the 30 μM AKG group and down-regulated gene list in the 750 μM AKG group (Fig. 4F, Table S1). Genes associated with this term included *TMEM126B*, *COX5B*, *NDUFS4*, *NDUFS9* and others (Fig. 4H). The changes in NDUFB9 expression at the protein level were consistent with those observed at the transcriptional level (Fig. 4G). These finding suggest that AKG affects oocyte mitochondrial function by regulating complex I.

The effects of AKG on cell-cell communication between cumulus cells and oocyte

Close intercellular communication between cumulus-oocytes is essential during oocyte maturation. The intensity of communication between cumulus cells and oocytes across different treatment groups was calculated using CellChat software package. The results demonstrated a significant increase in communication intensity between cumulus cells and oocytes in the 30 μM AKG group, whereas no significant difference was observed in the 750 μM AKG group compared to the control group (Fig. 5A). The similar trend was found in the GDF9

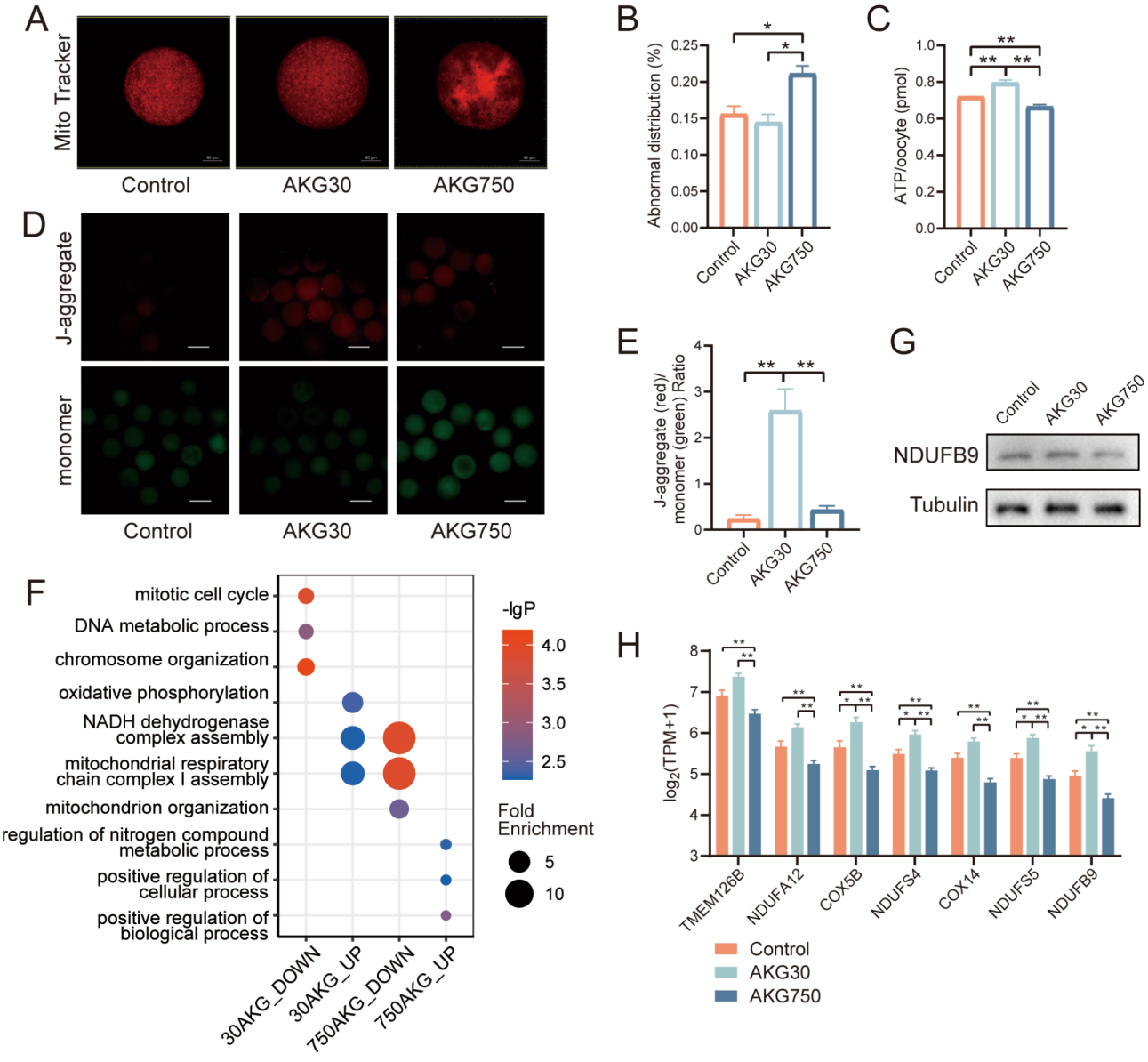

Fig. 4 Effect of AKG supplementation on oocyte mitochondrial distribution and function. (A) Representative images of mitochondria distribution labeled with MitoTracker Red, Scale bar = 40 μM. (B) The proportion of abnormally distributed mitochondria, $n = 30$. (C) Oocyte ATP levels, $n = 3$. (D) Representative images stained with JC-1 indicated MMP levels in control ($n = 27$), AKG30 ($n = 27$), and AKG750 ($n = 25$). (E) The statistical data from (D). (F) GO-BP pathway analysis of differential genes between both AKG concentrations vs. control group, color represents -lg(P-value), and circle size represents fold enrichment. (G) Immunoblotting of NDUFB9 in control, 30 μM AKG, and 750 μM AKG treated oocytes. (H) The expression of mitochondrial respiratory chain complex I related genes is expressed by $\log_2(\text{TPM} + 1)$, $n = 8$

pathway's communication intensity, as revealed by the ligand-receptor pair analysis (Fig. 5B), along with the GDF9 protein and transcript level in oocytes (Fig. 5C, D). Communications between oocytes and cumulus cells primarily depends on gap junction and transzonal projections (TZPs). Both communication pathways were evaluated. The intercellular gap junction was evaluated using Calcein-AM staining. The results showed that AKG treatments had no significant effect on gap junction communication compared to the control group (Fig. 5E). TZPs were labeled using F-actin fluorescence. The results showed that as the maturation of the COCs, the intensity of TZPs gradually reduced in the control group. The 750 μM AKG treatment had no significant impact, whereas the 30 μM AKG treatment significantly increased TZPs intensity at 15 h of incubation compared to control group (Fig. 5F, G).

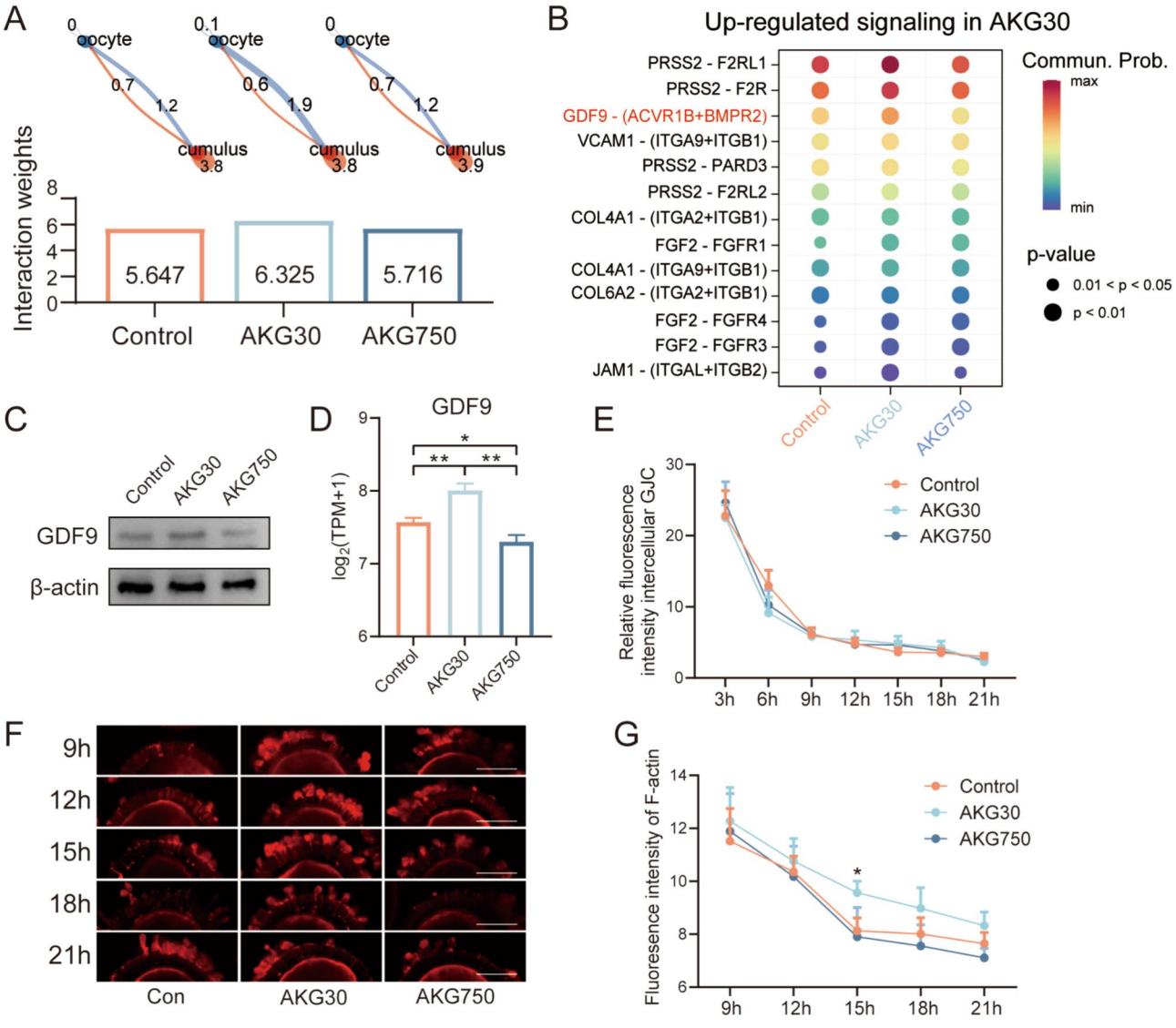

Fig. 5 Effect of AKG on cell-cell communication between cumulus and oocyte **(A)** The interaction weight plot of COCs. The thickness of the line indicates the number of interactions, and the stronger the interaction weight/intensity between the two cell types. Bar plot showed the total interaction weight of COCs in each group. **(B)** The up-regulated (increased) signaling ligand-receptor pairs were identified by comparing the communication probabilities in AKG30 samples and other samples. **(C)** Immunoblotting of GDF9 in control, 30 and 750 μM AKG treated oocytes. **(D)** The expression of GDF9 in oocytes, expressed using log2(TPM + 1), $n = 8$. **(E)** the fluorescence intensity of oocytes Calcein-AM to indicate the changes of Cumulus cell-oocyte gap junction permeability during oocyte maturation, $n = 9$. **(F)** Representative images of the fluorescence intensity of F-actin on the zona pellucida to indicate the changes of transzonal projections (TZPs) during oocyte maturation. **(G)** Line graph showed the changes of TZPs during oocyte maturation

Effects of AKG and GDF9 on cumulus cells expansion

Sequencing results showed that the expression of cumulus expansion-related genes, including *HAS2*, *PTX3*, *CD44* and *HMMR*, were not significantly altered in the 30 μM AKG treatment group but was significantly down-regulated in cumulus cells treated with 750 μM AKG compared to the control group (Fig. 6A). The changes in HAS2 expression at protein level were consistent with those observed at the transcriptional level (Fig. 6B). These findings further confirmed that 750 μM AKG significantly inhibited cumulus cell expansion. However, GDF9 supplementation reversed the suppressive effect of high concentration of AKG on cumulus expansion, as well as the expression of cumulus expansion-related genes, compared to the 750 μM AKG group alone (Fig. 6C-F).

Discussion

AKG has been shown to exhibit the beneficial effects on the in vitro oocyte maturation, but the exact mechanisms and especially, its potential risk at high dose remain to be clarified. Therefore, this study investigated the effects of various concentrations of AKG on COCs during IVM in dairy cows.

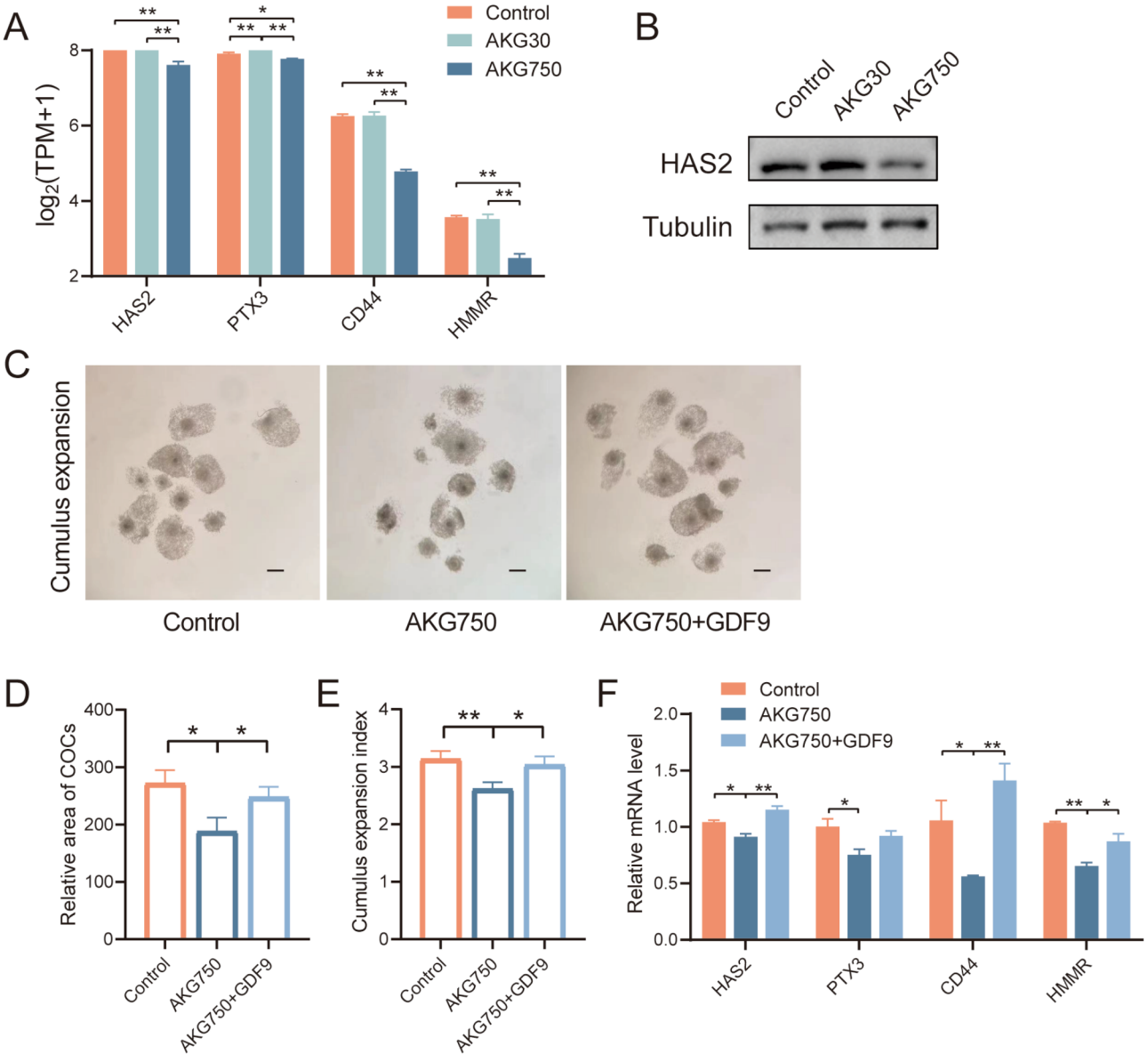

Fig. 6 Effects of AKG and GDF9 on cumulus cells expansion. **(A)** The expression of cumulus expansion related genes *HAS2*, *PTX3*, *CD44* and *HMMR* in cumulus cells expressed by $\log_2$ (TPM + 1), $n = 3$. **(B)** Immunoblotting of HAS2 in control, 30 and 750 μM AKG treated cumulus cells. **(C)** Representative images of the COCs after 22 h of culture, Scale bar = 200 μM, $n = 30$. (D) Relative cumulus expansion area $n = 30$. **(E)** Cumulus expansion index, $n = 30$. **(F)** qPCR results showed the expression of cumulus expansion related genes *HAS2*, *PTX3*, *CD44* and *HMMR* in cumulus, $n = 3$

The IVM process is more susceptible to oxidative stress compared to in vivo conditions. Our evidence revealed that AKG regulates the oxidative damage of cumulus cells and further supports the metabolic framework balance of oocyte development through gap junctions. As an antioxidant, AKG reacts directly with H_2O_2 to produce succinate, water, and CO_2 [35], thereby reducing ROS accumulation and GSH depletion in cumulus cells. Furthermore, the appropriate concentration of AKG upregulated the expressions of genes involved in GSH synthesis and GSSG recycling in cumulus cells, leading to increased GSH/GSSG and NADPH/NADP+ratios. Cumulus cells transport antioxidants, including GSH and NADPH, to oocytes through cumulus-oocyte gap junctions and TZPs. GSH is the primary intracellular antioxidant and reductant [9], its continuously supplied by cumulus cells, thereby further reducing oxidative stress and apoptosis in the oocytes.

Oocyte quality is closely linked to mitochondrial function, with mitochondria serving as a primary target of AKG. Our results showed that AKG at 30 μM upregulated the expression of complex I associated genes, resulting in elevated MMP and ATP production in oocytes. We speculate that as an important intermediate

of TCA cycle, exogenous addition of AKG enhances TCA cycle flux and ATP production. Enhanced oocyte metabolism likely impacts intercellular communication within COCs. Cell communication analysis showed that AKG at 30 μM significantly enhanced communication from oocytes to cumulus cells, especially the expression of oocyte-secreted factors (OSFs) such as GDF9. The absence of oocyte-derived GDF9 transport could compromise cumulus cell growth. Additionally, cytoplasmic extensions of cumulus cells, TZPs, were also significantly enhanced.

Physiological concentrations of AKG in follicular fluid of different species vary widely, ranging from 48 to 80 μM in human, 5 to 10μM in pigs [21], 1–5 μM in cows (unpublished data). Furthermore, physiological AKG concentration gradually decreases with age [36]. Several studies have reported the beneficial effects of AKG on oocyte maturation, with the concentrations of AKG used in these studies are close to physiological range [21, 22, 37]. As an intermediary of energy metabolism, excessive concentration of AKG will inevitably generate the negative feedback on energy metabolism. For example, AKG accumulation leads to a synchronous increase in the expression of OGDH. OGDH is a constituent of ketoglutarate dehydrogenase (KGDH), which degrades AKG and produces ROS and NADH at a high rate [38]. KGDH plays a key role in controlling flux through the TCA cycle and is the rate limiting enzyme for NADH production [39]. The increased NADH production, in turn, limits the rate of electron transport and ATP synthesis, and in extreme cases, elevated AKG levels can impair mitochondrial function [40]. However, to our knowledge, few studies have investigated the potential risk of high concentrations of AKG on reproductive physiology [21, 40].

In this study, 750 μM of AKG was selected which exceeds the physiological concentration (5 μM) by more than 150 folds. The results showed that this high concentration not only lacked protective effects but also significantly impaired the process of oocyte IVM. This included the inhibition of cumulus cell expansion and reduction of oocyte quality. High levels of AKG inhibited the energy metabolism of COCs, leading to increased ROS production, abnormal mitochondrial distribution, and impaired communication between cumulus cell and oocytes. One of the most notable alteration caused by high level AKG was the downregulated gene expression of GDF9. GDF9 induces the expression of key genes in cumulus cells, such as Hyaluronan Synthase 2 (*HAS2*), Cyclooxygenase 2 (*COX2*), Pentraxin 3 (*PTX3*), Prostaglandin-Endoperoxide Synthase 2 (*PTGS2*), and Gremlin1 (*GREM1*), which are essential for cumulus expansion during oocyte maturation prior to ovulation [41, 42]. The reduction in GDF9 expression appears to play a critical role in the negative effects of high level of AKG on cumulus expansion during IVM. Notably, supplementation with GDF9 almost completely reversed the adverse effects of high AKG concentrations on cumulus expansion and the expression of related genes (Fig. 6). These findings align with previous reports in which the pyruvate uptake inhibitor UK5099 suppressed the GDF9 expression in oocytes, inhibiting folliculogenesis, with GDF9 supplementation rescuing these processes [43].

In conclusion, this study explored the concentration dependent effects of AKG on COCs during IVM. The results showed that an appropriate concentration of AKG enhances cumulus expansion, cumulus-oocyte communication, oocyte quality, and embryo development in vitro. These effects are primarily mediated by AKG's role in regulating the redox balance between cumulus cells and oocytes. However, excessively high concentration of AKG had detrimental effects on these parameters. This study provides novel insights into the negative impact of high AKG concentrations on reproductive physiology, a phenomenon not previously reported, and offers valuable guidance for selecting AKG concentrations in future oocyte IVM research.

Supplementary Information

The online version contains supplementary material available at https://doi.org/10.1186/s12964-024-01827-z.

Supplementary Material 1: Effect of AKG treated oocyte on embryo development. (A) Representative images of blastocysts at the 8th day of IVF developed from oocytes treated with different concentrations of AKG during maturation. Scale bar = 150 μM. (B) Cleavage rate at 2 days after IVF. The number inside each bar represents the number of cleavage embryos / all embryos. Data were analyzed using the Chi-squared test with SPSS. (C) Blastocyst development rate (blastocyst rate = number of blastocysts / number of cleavages) at the 8th day of IVF. The number inside the bars represents the number of blastocyst embryos/ cleavage embryos. Data were analyzed using the Chi-squared test with SPSS. (D) Representative images of immunofluorescence staining showing the number of cells in the blastocyst inner cell mass labeled with Sox2. Scale bar = 70 μM, $n = 21$ (control), $n = 20$ (AKG30), $n = 22$ (AKG150), $n = 21$ (AKG750). (E) Number of inner cell mass (ICM) cells in blastocysts. (F) Total cell number of blastocysts. (J) Number of trophoblast (TE) cell in blastocysts, TE cell number = Total cell number – ICM cell number. (H) Number of inner cell mass/ TE cells in blastocyst

Supplementary Material 2

Supplementary Material 3

Author contributions

Yunjie Liu: Writing – review & editing, Writing – original draft, Visualization, Software, Formal analysis, Data curation, Conceptualization. Xin Xiao: Visualization, Formal analysis, Data curation. Likai Wang: Visualization, Formal analysis, Data curation. Yao Fu: Visualization, Formal analysis, Data curation. Songyang Yao: Supervision, Data curation. Xuening Liu: Data curation. Boda Chen: Software. Jiarui Gao: Data curation. Yaying Zhai: Data curation. Zixia Shen: Data curation. Laiqing Yan: Data curation. Yiwei Wang: Data curation. Pengyun Ji: Supervision, Data curation. Bingyuan Wang: Supervision, Data curation. Guoshi Liu: Writing – review & editing, Resources, Project administration, Funding acquisition, Conceptualization.

Funding
This work was supported in part by the Agricultural Biological Breeding Major Project, grant number 2023ZD04049.

Data availability
All data used during the current study are available from the corresponding author on reasonable request.

Declarations

Competing interests
The authors declare no competing interests.

Author details
[1]State Key Laboratory of Animal Biotech Breeding, Key Laboratory of Animal Genetics and Breeding of the Ministry of Agricultural, Beijing Key Laboratory for Animal Genetic Improvement, College of Animal Science and Technology, China Agricultural University, No. 2 Yuanmingyuan West road, Beijing 100193, China

Received: 1 July 2024 / Accepted: 13 September 2024
Published online: 03 October 2024

References

1. De Geyter C, Wyns C, Calhaz-Jorge C, de Mouzon J, Ferraretti AP, Kupka M, et al. 20 years of the European IVF-monitoring Consortium registry: what have we learned? A comparison with registries from two other regions. Hum Reprod. 2020;35(12):2832–49.
2. Joao HM, Viana C. 2022 Statistics of embryo production and transfer in domestic farm animals. Embryo Technology Newsletter. 2023;41(4).
3. Agarwal A, Maldonado RI, Anagnostopoulou C, Cannarella R, Boitrelle F, Munoz LV et al. Oxidative stress and assisted Reproduction: a Comprehensive Review of its pathophysiological role and strategies for optimizing embryo culture environment. Antioxid (Basel). 2022;11(3).
4. Arias-Alvarez M, Garcia-Garcia RM, Lopez-Tello J, Rebollar PG, Gutierrez-Adan A, Lorenzo PL. In vivo and in vitro maturation of rabbit oocytes differently affects the gene expression profile, mitochondrial distribution, apoptosis and early embryo development. Reprod Fertil Dev. 2017;29(9):1667–79.
5. Richani D, Dunning KR, Thompson JG, Gilchrist RB. Metabolic co-dependence of the oocyte and cumulus cells: essential role in determining oocyte developmental competence. Hum Reprod Update. 2021;27(1):27–47.
6. von Mengden L, Klamt F, Smitz J. Redox Biology of Human Cumulus Cells: Basic concepts, Impact on Oocyte Quality, and potential clinical use. Antioxid Redox Signal. 2020;32(8):522–35.
7. Xie J, Xu X, Liu S. Intercellular communication in the cumulus-oocyte complex during folliculogenesis: a review. Front Cell Dev Biol. 2023;11:1087612.
8. Martinez CA, Rizos D, Rodriguez-Martinez H, Funahashi H. Oocyte-cumulus cells crosstalk: new comparative insights. Theriogenology. 2023;205:87–93.
9. Aquilano K, Baldelli S, Cardaci S, Rotilio G, Ciriolo MR. Nitric oxide is the primary mediator of cytotoxicity induced by GSH depletion in neuronal cells. J Cell Sci. 2011;124(Pt 7):1043–54.
10. Liu T, Sun L, Zhang Y, Wang Y, Zheng J. Imbalanced GSH/ROS and sequential cell death. J Biochem Mol Toxicol. 2022;36(1):e22942.
11. Ghosh D, Levault KR, Brewer GJ. Relative importance of redox buffers GSH and NAD(P)H in age-related neurodegeneration and Alzheimer disease-like mouse neurons. Aging Cell. 2014;13(4):631–40.
12. Elvin JA, Yan C, Matzuk MM. Growth differentiation factor-9 stimulates progesterone synthesis in granulosa cells via a prostaglandin E2/EP2 receptor pathway. Proc Natl Acad Sci U S A. 2000;97(18):10288–93.
13. Sasseville M, Ritter LJ, Nguyen TM, Liu F, Mottershead DG, Russell DL, et al. Growth differentiation factor 9 signaling requires ERK1/2 activity in mouse granulosa and cumulus cells. J Cell Sci. 2010;123(Pt 18):3166–76.
14. Sugiura K, Su YQ, Diaz FJ, Pangas SA, Sharma S, Wigglesworth K, et al. Oocyte-derived BMP15 and FGFs cooperate to promote glycolysis in cumulus cells. Development. 2007;134(14):2593–603.
15. Gyanwali B, Lim ZX, Soh J, Lim C, Guan SP, Goh J, et al. Alpha-ketoglutarate dietary supplementation to improve health in humans. Trends Endocrinol Metab. 2022;33(2):136–46.
16. Asadi SA, Edgar D, Liao CY, Hsu YM, Lucanic M, Asadi SA, et al. Alpha-Ketoglutarate, an endogenous metabolite, extends Lifespan and compresses Morbidity in Aging mice. Cell Metab. 2020;32(3):447–56.
17. Yang Y, He P, Hou Y, Liu Z, Zhang X, Li N. Osmundacetone modulates mitochondrial metabolism in non-small cell lung cancer cells by hijacking the glutamine/glutamate/alpha-KG metabolic axis. Phytomedicine. 2022;100:154075.
18. Liu L, Zhang W, Liu T, Tan Y, Chen C, Zhao J, et al. The physiological metabolite alpha-ketoglutarate ameliorates osteoarthritis by regulating mitophagy and oxidative stress. Redox Biol. 2023;62:102663.
19. Read CC, Edwards L, Schrick N, Rhinehart JD, Payton RR, Campagna SR, et al. Correlation between pre-ovulatory follicle diameter and follicular fluid metabolome profiles in Lactating Beef cows. Metabolites. 2021;11(9):623.
20. Atkins JA, Smith MF, MacNeil MD, Jinks EM, Abreu FM, Alexander LJ, et al. Pregnancy establishment and maintenance in cattle. J Anim Sci. 2013;91(2):722–33.
21. Zhang Z, He C, Gao Y, Zhang L, Song Y, Zhu T, et al. Alpha-ketoglutarate delays age-related fertility decline in mammals. Aging Cell. 2021;20(2):e13291.
22. Wang H, Xu J, Li H, Chen W, Zeng X, Sun Y, et al. Alpha-ketoglutarate supplementation ameliorates ovarian reserve and oocyte quality decline with aging in mice. Mol Cell Endocrinol. 2023;571:111935.
23. Chu M, Yao F, Xi G, Yang J, Zhang Z, Yang Q, et al. Vitamin C rescues in vitro Embryonic Development by correcting impaired active DNA demethylation. Front Cell Dev Biol. 2021;9:784244.
24. Hao Y, Wang J, Ren J, Liu Z, Bai Z, Liu G, et al. Effect of dimethyl alpha-ketoglutarate supplementation on the in vitro developmental competences of ovine oocytes. Theriogenology. 2022;184:171–84.
25. FUNSHO FAGBOHUN C, DOWNS SM. Maturation of the mouse oocyte-cumulus cell complex: stimulation by lectins. Biol Reprod. 1990;42(3):413–23.
26. Thomas RE, Armstrong DT, Gilchrist RB. Bovine cumulus cell-oocyte gap junctional communication during in vitro maturation in response to manipulation of cell-specific cyclic adenosine 3',5'-monophosphate levels. Biol Reprod. 2004;70(3):548–56.
27. Macaulay AD, Gilbert I, Caballero J, Barreto R, Fournier E, Tossou P, et al. The gametic synapse: RNA transfer to the bovine oocyte. Biol Reprod. 2014;91(4):90.
28. Chen S, Zhou Y, Chen Y, Gu J. Fastp: an ultra-fast all-in-one FASTQ preprocessor. Bioinformatics. 2018;34(17):i884–90.
29. Andrews S, FastQC. A Quality Control Tool for High Throughput Sequence Data [Online]. 2010. http://www.bioinformatics.babraham.ac.uk/projects/fastqc/. Accessed.
30. Dobin A, Davis CA, Schlesinger F, Drenkow J, Zaleski C, Jha S, et al. STAR: ultrafast universal RNA-seq aligner. Bioinformatics. 2013;29(1):15–21.
31. Liao Y, Smyth GK, Shi W. The subread aligner: fast, accurate and scalable read mapping by seed-and-vote. Nucleic Acids Res. 2013;41(10):e108.
32. Love MI, Huber W, Anders S. Moderated estimation of Fold change and dispersion for RNA-seq data with DESeq2. Genome Biol. 2014;15(12):550.
33. Reimand J, Kull M, Peterson H, Hansen J, Vilo J. G:Profiler–a web-based toolset for functional profiling of gene lists from large-scale experiments. Nucleic Acids Res. 2007;35(Web Server issue):W193–200.
34. Jin S, Guerrero-Juarez CF, Zhang L, Chang I, Ramos R, Kuan CH, et al. Inference and analysis of cell-cell communication using CellChat. Nat Commun. 2021;12(1):1088.
35. He L, Wu J, Tang W, Zhou X, Lin Q, Luo F, et al. Prevention of oxidative stress by alpha-ketoglutarate via activation of CAR Signaling and Modulation of the expression of key antioxidant-Associated targets in Vivo and in Vitro. J Agric Food Chem. 2018;66(43):11273–83.
36. Tian Q, Zhao J, Yang Q, Wang B, Deavila JM, Zhu MJ, et al. Dietary alpha-ketoglutarate promotes beige adipogenesis and prevents obesity in middle-aged mice. Aging Cell. 2020;19(1):e13059.
37. Chen Q, Gao L, Li J, Yuan Y, Wang R, Tian Y et al. Alpha-ketoglutarate improves meiotic maturation of porcine oocytes and promotes the development of PA Embryos, potentially by reducing oxidative stress through the Nrf2 pathway. Oxid Med Cell Longev. 2022:7113793.
38. Quinlan CL, Goncalves RL, Hey-Mogensen M, Yadava N, Bunik VI, Brand MD. The 2-oxoacid dehydrogenase complexes in mitochondria can produce superoxide/hydrogen peroxide at much higher rates than complex I. J Biol Chem. 2014;289(12):8312–25.
39. Tretter L, Adam-Vizi V. Inhibition of Krebs cycle enzymes by hydrogen peroxide: a key role of [alpha]-ketoglutarate dehydrogenase in limiting NADH production under oxidative stress. J Neurosci. 2000;20(24):8972–9.

40. Lomenick B, Hao R, Jonai N, Chin RM, Aghajan M, Warburton S, et al. Target identification using drug affinity responsive target stability (DARTS). Proc Natl Acad Sci U S A. 2009;106(51):21984–9.
41. Pangas SA, Matzuk MM. The art and artifact of GDF9 activity: cumulus expansion and the cumulus expansion-enabling factor. Biol Reprod. 2005;73(4):582–5.
42. Elvin JA, Clark AT, Wang P, Wolfman NM, Matzuk MM. Paracrine actions of growth differentiation factor-9 in the mammalian ovary. Mol Endocrinol. 1999;13(6):1035–48.
43. Tanaka K, Hayashi Y, Takehara A, Ito-Matsuoka Y, Tachibana M, Yaegashi N, et al. Abnormal early folliculogenesis due to impeded pyruvate metabolism in mouse oocytesdagger. Biol Reprod. 2021;105(1):64–75.

Publisher's note